Asymptotic Behavior of Localization and Sensing in the Near Field of Extremely Large Aperture Arrays

Asymptotic Behavior of Localization and Sensing in the Near Field of Extremely Large Aperture Arrays

Caterina Giovannetti*†‡, Nicolò Decarli*‡, Alberto Zanella*‡, Davide Dardari†‡

* IEIIT, National Research Council (CNR), 40136 Bologna, Italy
† DEI, Università di Bologna, 40136 Bologna, Italy
‡ National Laboratory of Wireless Communications (WiLab), CNIT, 40136 Bologna, Italy

***Abstract*—This paper investigates the asymptotic behavior of localization and sensing accuracy in the near field of extremely large aperture arrays. By accounting for the wavefront curvature and the amplitude variations inherent in the near-field regime, we examine how fundamental limits, such as the Cramér-Rao lower bound, evolve as array apertures grow to extreme scales. Our analysis characterizes the interplay between geometry and signal parameters, and derives asymptotic expressions for localization and sensing accuracy, revealing scaling laws distinct from those in conventional far- and near-field scenarios. Through the proposed analytical and numerical analysis, it is shown that traditional near-field results fail when the array size becomes comparable to the target distance (geometric near-field condition).**

I. Introduction

The upcoming era of sixth generation (6G) wireless networks envisions a transformative integration of communication, localization, and sensing into a unified system, enabling a broad range of applications such as autonomous vehicles, augmented reality, and industrial automation. Beyond delivering ultra-reliable and low-latency communication, 6G aims to provide precise environmental awareness and user localization, often with sub-centimeter accuracy, to support increasingly complex and interconnected use cases. This convergence of communication and sensing technologies introduces new opportunities for communication systems, enabling simultaneous data transmission, localization, and environmental mapping through shared hardware and spectrum resources [1].

Central to achieving these goals is the exploitation of near-field propagation phenomena, particularly when using large antenna arrays. Unlike traditional far-field systems, where the planar wavefront assumptions dominate, near-field systems operate in a regime where spherical wavefronts and spatial signal variations become prominent. These effects are especially pronounced with the emergence of extremely large aperture arrays (ELAAs), which promise to push the boundaries of localization and sensing precision [2]. ELAAs, characterized by aperture sizes even comparable to or exceeding the transmitter-receiver (for localization) or transceiver-target (for radar-based sensing) distance, offer the potential for unprecedented resolution by capturing fine-grained spatial information. Examples are the so-called *radio stripes*, recently introduced as possible cell-free multiple input multiple output (MIMO) implementations [3].

ELAAs also introduce fundamental challenges that demand a reevaluation of traditional models and performance limits. In communication, for example, classical models for path loss scaling laws and the number of available communication modes fail when the array size approaches the transmitter-receiver distance [4]. These deviations lead to novel phenomena that redefine the limits of system capacity and efficiency. Although the impact of these effects on communication has been widely studied in the last years [4]–[6], their implications for localization and sensing remain less understood. Performance limits for near-field distance estimation are analyzed, for example, in [7] where it is shown that accuracy enhances as the aperture increases; specifically, the Cramér-Rao lower bound (CRLB) for near-field distance estimation scales inversely with the fourth power of the array aperture. Similarly, it is recognized that the accuracy of angle estimation enhances as the aperture increases and depends on the angle, but not on the distance [7]. Some very recent studies showed that different behaviors can be obtained when ELAAs are adopted in conjunction with MIMO radar configurations [8], [9]; however, the impact of the amplitude variations across the array are usually not theoretically investigated, and the active localization case is not considered.

This paper explores the performance limits of near-field localization and sensing using ELAAs. We demonstrate that both distance and angle estimation accuracies cannot grow unbounded as predicted when traditional near-field models are adopted, and saturation effects in the performance arise as the size of the array grows. Importantly, the underlying mechanisms driving these limitations are different for the two types of measurements (distance and angle). Specifically, we show that for distance estimation, the saturation arises mainly from the phase distribution across the array elements. In contrast, angle estimation accuracy saturates because of the nonuniform signal strength across the array elements. By systematically analyzing these near-field phenomena in the presence of ELAAs, this work bridges the gap between theoretical modeling and practical performance limits in near-field localization and sensing applications.

This work was supported by the European Union under the Italian National Recovery and Resilience Plan (NRRP) of NextGenerationEU, partnership on "Telecommunications of the Future" (PE00000001 - program "RESTART"), and by the EU HORIZON-JU-SNS-2022 project TIMES (Grant no. 101096307).

II. System Model

In this section we describe the transmitted signal model for localization and sensing in the near field of an ELAA, the geometry of the scenario and the received signal model. Let us consider in the following two cases:

(a) Localization of a single-antenna user equipment (UE) using a base station (BS) equipped with an ELAA of K elements;
(b) Sensing of a passive target using a single input multiple output (SIMO) monostatic radar at the BS, thus with a single transmitting antenna and K receiving elements.

We consider the antennas at the BS organized as a uniform linear ELAA and 2D localization/sensing. Without loss of generality, assume that K is odd. Accordingly, the array aperture is defined as $D_{\text{elaa}} = (K-1)\,\delta$, where δ denotes the antenna spacing. The reference system is placed with the origin corresponding to the central element of the ELAA at the BS, which is oriented along the x axis (see Fig. 1). Denote with $\tilde{\mathbf{p}}_k = [x_k, y_k]^\top$ the position of the k-th receiving antenna at the BS , for $k = -(K-1)/2, \ldots, (K-1)/2$, so that $y_k = 0, \forall k$, and $x_0 = 0$. For case (a) of localization, we assume the transmitting UE placed in position $\tilde{\mathbf{p}} = [x, y]^\top$. For case (b) of sensing, we assume a point target placed in position $\tilde{\mathbf{p}} = [x, y]^\top$. For convenience, let us now consider a polar coordinate system. In this case, we can write the position of the UE/target as $\mathbf{p} = [\theta, d]^\top$ where θ denotes the angle with respect to the broadside direction of the receiving ELAA (i.e., the angle of arrival (AoA) of the signal received at the BS), and d denotes the distance between the UE/target and the central element of the receiving ELAA at the BS (i.e., the reference antenna), that is

$$d = \sqrt{x^2 + y^2}, \qquad \theta = \operatorname{atan}\left(\frac{x}{y}\right) \tag{1}$$

where $\operatorname{atan}(\cdot)$ is the four-quadrant inverse tangent. We denote by d_k the distance between the UE/target and the k-th receiving antenna that can be expressed as

$$d_k = \|\tilde{\mathbf{p}} - \tilde{\mathbf{p}}_k\| = \sqrt{(x - x_k)^2 + y^2}\,. \tag{2}$$

Adopting the polar coordinate system, we can write

$$\begin{aligned} d_k &= \sqrt{d^2 \sin^2\theta + x_k^2 - 2x_k d \sin\theta + d^2\cos^2\theta} \\ &= d\sqrt{1 + \frac{x_k^2}{d^2} - \frac{2x_k \sin\theta}{d}}. \end{aligned} \tag{3}$$

When considering case (a) of localization, the UE transmits an uplink data packet spanning N subcarriers of an orthogonal frequency-division multiplexing (OFDM) signal. Focusing on a single symbol, the transmitted OFDM waveform, in complex baseband, can be written as

$$s(t) = \sum_n \sqrt{P}\, x_n e^{\mathrm{j}2\pi n \Delta f t}\, \text{rect}\left(\frac{t}{T_{\text{sym}}}\right) \tag{4}$$

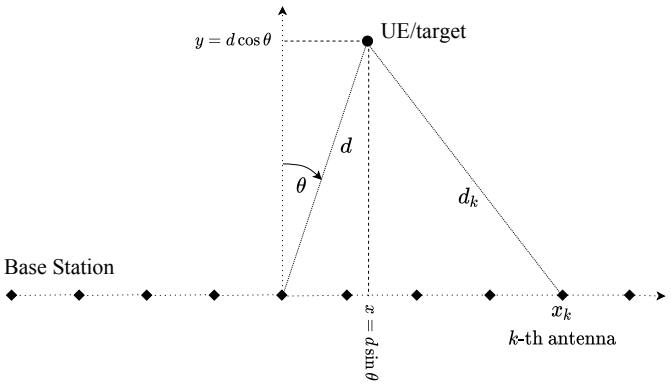

Fig. 1. Considered 2D scenario, where an ELAA is employed to localize a single antenna transmitting UE or to sense a passive point target in $\mathbf{p} = [\theta, d]$.

where $P = P_{\text{T}}/N$ is the power allocated to each subcarrier, P_{T} is the total transmit power, and x_n is the data symbol (e.g., a pilot used for channel estimation and localization) transmitted in the n-th subcarrier with $\mathbb{E}\{|x_n|^2\} = 1$, for $n = -(N-1)/2, \ldots, (N-1)/2$. The symbol time is $T_{\text{sym}} = T + T_{\text{cp}}$ where T_{cp} stands for the cyclic prefix duration and $T = 1/\Delta f$, with Δf indicating the subcarrier spacing. The bandpass signal transmitted by the UE is

$$\tilde{s}(t) = \Re\left\{s(t)\, e^{\mathrm{j}2\pi f_{\text{c}} t}\right\} \tag{5}$$

where f_{c} is the carrier frequency.

When considering case (b) of sensing, the central element of the BS transmits the signal (5) according to its baseband (4). This signal is then reflected by the target in position $\mathbf{p}$, and all antenna elements of the BS receive the signal, as for the active localization case (SIMO radar).

The BS aims at estimating the distance $d = ||\tilde{\mathbf{p}}||$ (i.e., the *range*) and the angle θ (i.e., the AoA) processing the signal received at its ELAA. After standard cyclic prefix removal and fast Fourier transform (FFT) processing, the received signal for a given OFDM symbol, in complex baseband, can be written as [10]

$$r_{n,k} = y_{n,k} + z_{n,k} = \sqrt{P}\, x_n \beta_{n,k}\, e^{-\mathrm{j}2\pi f_n \tau_k} e^{\mathrm{j}\varphi} + z_{n,k} \tag{6}$$

where $f_n \triangleq f_{\text{c}} + n\Delta f$ is the frequency associated with the n-th subcarrier, φ accounts for the phase synchronization mismatch between the transmitter and the receiver,[1] $\beta_{n,k}$ are the channel scaling coefficients. The term τ_k denotes the time taken by the signal to travel between the UE and the k-th BS antenna (for localization) or between the transmitting antenna, the target and the k-th BS antenna (for sensing). The term $z_{n,k}$ denotes the additive white Gaussian noise (AWGN), with $z_{n,k} \sim \mathcal{CN}(0, \sigma^2)$.

Assuming a small bandwidth[2] we have $f_n \approx f_{\text{c}}$, and the channel scaling coefficients can be considered constant on the

[1] For the sensing case, we could have $\varphi = 0$ if the receiver is phase-synchronized with the co-located transmitter.

[2] An analysis for wideband OFDM signals can be found in [8].

different subcarriers, i.e., $\beta_{n,k} = \beta_k \ \forall n$. The signal-to-noise ratio (SNR) at the k-th receiving antenna can be expressed as $\mathsf{SNR}_k = P\beta_k^2/\sigma^2 = \alpha_k^2/\sigma^2$. The channel scaling coefficients for localization (a) and sensing (b) are given by the Friis laws in the active and passive case, that are, respectively

$$\beta_k^{2(\mathrm{loc})} = \frac{G_{\mathrm{T}} G_{\mathrm{R}} \lambda^2}{(4\pi d_k)^2}, \qquad \beta_k^{2(\mathrm{sens})} = \frac{G_{\mathrm{T}} G_{\mathrm{R}} \lambda^2 \rho}{(4\pi)^3 d^2 d_k^2} \tag{7}$$

where G_{T} and G_{R} are the transmitting and receiving antenna gains, $\lambda = c/f_{\mathrm{c}}$ is the wavelength, c is the speed of light, and ρ is the radar cross section (RCS) of the target.

When $d > D_{\mathrm{elaa}}$, the channel coefficients can be considered almost equal across the array, leading to $\beta_{n,k} = \beta$, $\forall n, k$. For $d < D_{\mathrm{elaa}}$, instead, this approximation is no longer valid. Indeed, it is necessary to compute the path loss at each antenna element, because d_k can change significantly across the array aperture. Starting from (7) and using (3), the corresponding SNR at the k-th antenna can be written for the two cases as

$$\mathsf{SNR}_k^{(\mathrm{loc})} = \frac{P\, G_{\mathrm{T}} G_{\mathrm{R}} \lambda^2}{(4\pi)^2 d^2 \sigma^2} \frac{1}{\left(1 + \frac{x_k^2}{d^2} - \frac{2x_k \sin\theta}{d}\right)} = \frac{\mathsf{SNR}_0}{f_k} \tag{8}$$

$$\mathsf{SNR}_k^{(\mathrm{sens})} = \frac{P\, G_{\mathrm{T}} G_{\mathrm{R}} \lambda^2 \rho}{(4\pi)^3 d^4 \sigma^2} \frac{1}{\left(1 + \frac{x_k^2}{d^2} - \frac{2x_k \sin\theta}{d}\right)} = \frac{\mathsf{SNR}_0}{f_k} \tag{9}$$

where $\mathsf{SNR}_0 = P\beta_0^2/\sigma^2$ is the SNR at the reference antenna in the localization/sensing case and

$$f_k = 1 + \frac{x_k^2}{d^2} - \frac{2x_k \sin\theta}{d}. \tag{10}$$

Thus, $\beta_k^2 = \beta_0^2/f_k$ and from (8) and (9) the resulting SNR is the scaled version of that at the reference antenna. Moreover, once defined the SNR at the reference antenna, no differences are experienced between localization and sensing for the SNR scaling law across the array aperture.

For what concerns the time displacement parameter across the array τ_k, for localization (a) we have $\tau_k = d_k/c$, while for sensing (b) $\tau_k = (d + d_k)/c$, considering the transmitter synchronized in time with the receiver.[3] Notice that, for sensing (b), we can incorporate the phase shift due to the forward path between the transmitting antenna and the target within the common phase term φ. Therefore, hereafter we no longer make a distinction between localization and sensing by considering always $\tau_k = d_k/c = d\sqrt{f_k}/c$. Since the transmitted symbols are known by the receiver and used as pilots, we set $x_n = 1$. Thus, for the sake of performance limits derivation, we consider the received signal model

$$r_{n,k} = y_{n,k} + z_{n,k} = \frac{\alpha}{\sqrt{f_k}} e^{-\frac{\mathrm{j}2\pi f_{\mathrm{c}} d\sqrt{f_k(\mathbf{p})}}{c}} e^{\mathrm{j}\varphi} + z_{n,k} \tag{11}$$

where $\alpha = \sqrt{P}\beta_0$ and we have highlighted the dependence on $\mathbf{p} = [\theta, d]$ for the phase at each antenna.

[3]For the case of localization, this can be equivalently obtained by exploiting round trip time (RTT) measurements (e.g., through two-way ranging techniques), or differential measurements (e.g., time-difference-of-arrival (TDoA) techniques). For sensing, time synchronization can be easily realized thanks to the monostatic configuration considered.

III. Performance Limits

We now evaluate the performance limits for the estimation of the range d and AoA θ by exploiting the information coming from the phase shifts across the antenna elements in near-field conditions. To this end, we compute the CRLB for the set of parameters $\boldsymbol{\Theta} = \{d, \theta, \varphi, \alpha\}$ in (11). The (i, j) element of the Fisher information matrix (FIM) can be obtained as [11]

$$[\mathbf{J}]_{i,j} = \frac{2}{\sigma^2} \Re\left\{ \sum_n \sum_k \left[\frac{\partial y_{n,k}}{\partial \boldsymbol{\Theta}_i}\right]^* \left[\frac{\partial y_{n,k}}{\partial \boldsymbol{\Theta}_j}\right] \right\} \tag{12}$$

where $y_{n,k}$ is the noise-free version of $r_{n,k}$ in (11), leading to a 4×4 FIM in the form

$$\mathbf{J} = \left[\begin{array}{cc:cc} J_{dd} & J_{d\theta} & J_{d\varphi} & J_{d\alpha} \\ J_{\theta d} & J_{\theta\theta} & J_{\theta\varphi} & J_{\theta\alpha} \\ \hdashline J_{\varphi d} & J_{\varphi\theta} & J_{\varphi\varphi} & J_{\varphi\alpha} \\ J_{\alpha d} & J_{\alpha\theta} & J_{\alpha\varphi} & J_{\alpha\alpha} \end{array}\right] = \begin{bmatrix} \mathbf{J}_A & \mathbf{J}_B \\ \mathbf{J}_B^{\mathrm{T}} & \mathbf{J}_C \end{bmatrix} \tag{13}$$

since $J_{d\theta} = J_{\theta d}$, $J_{d\varphi} = J_{\varphi d}$, $J_{d\alpha} = J_{\alpha d}$, $J_{\varphi\theta} = J_{\theta\varphi}$, $J_{\alpha\theta} = J_{\theta\alpha}$, $J_{\alpha\varphi} = J_{\varphi\alpha}$.

To obtain the inverse $\mathbf{J}^{-1}$ of the FIM and compute the CRLB for the range d and AoA θ, thanks to its block form, we exploit the matrix inversion lemma. In this manner, the inverse sub-matrix related to the parameters of interest (i.e., d and θ) is obtained, reducing the computation complexity. Specifically, we have

$$\mathbf{J}_{1:2,1:2}^{-1} = \mathbf{H}^{-1} \tag{14}$$

where $\mathbf{H} \triangleq \mathbf{J}_A - \mathbf{J}_B \mathbf{J}_C^{-1} \mathbf{J}_B^{\mathrm{T}}$, that allows to take into account matrices with lower dimensions. Thus, we have the CRLB for near-field range and AoA estimation given by, respectively:

$$\mathsf{CRLB}^{(\hat{d})} = \mathbf{J}_{1,1}^{-1}, \qquad \mathsf{CRLB}^{(\hat{\theta})} = \mathbf{J}_{2,2}^{-1}. \tag{15}$$

A. Bounds in the Near-Field Region

The received signal in (11) presents a phase term dependent on d_k (thus, d and θ) through τ_k where $f_k(\mathbf{p}) = f_k(\theta, d)$ represents the wavefront curvature information [12]. To derive the performance bounds in the near-field region, two main assumptions are usually carried out [13]:

1) To simplify the strong nonlinearity of the phase profile in the near-field regime according to (11), the Fresnel approximation is exploited;
2) The amplitude variations across the array are neglected, by considering a constant SNR for all the K receiving antennas, i.e., $\alpha_k = \alpha \ \forall k$ (namely, $f_k = 1$ for the amplitude term in (11)).

The Fresnel approximation is based on the binomial expansion $\sqrt{1+b} \approx 1 + \frac{1}{2}b - \frac{1}{8}b^2 + ...$, considering $b = \frac{x_k^2}{d^2} - \frac{2x_k \sin\theta}{d}$. Applying the second-order approximation and then neglecting the terms above the second order, we have

$$d_k \approx d + \frac{x_k^2}{2d}\left(1 - \sin^2\theta\right) - x_k \sin\theta = d + \frac{x_k^2 \cos^2\theta}{2d} - x_k \sin\theta. \tag{16}$$

Thanks to the simplifications introduced by the Fresnel approximation and the constant path loss assumption, the closed-form expressions of the CRLBs for range and AoA estimation, respectively, are obtained as [7]

$$\mathsf{CRLB}^{(\hat{d})} = \frac{6c^2d^2\left(\delta^2\left(K^2-4\right)\sin^2\theta+15d^2\right)}{\pi^2 f_c^2 NK\,\mathsf{SNR}_0\cos^4\theta\,\delta^4\left(K^2-4\right)\left(K^2-1\right)}, \quad (17)$$

$$\mathsf{CRLB}^{(\hat{\theta})} = \frac{3c^2}{2\pi^2 f_c^2 NK\,\mathsf{SNR}_0\cos^2\theta\,\delta^2(K^2-1)}. \quad (18)$$

Considering large K and $\theta = 0$, we have

$$\mathsf{CRLB}^{(\hat{d})} \approx \frac{90\lambda^2 d^4}{\pi^2 NK\,\mathsf{SNR}_0\,D_{\text{elaa}}^4}, \quad (19)$$

$$\mathsf{CRLB}^{(\hat{\theta})} \approx \frac{3\lambda^2}{2\pi^2 NK\,\mathsf{SNR}_0\,D_{\text{elaa}}^2} \quad (20)$$

where it is shown that the lower bound for the variance of the range estimation accuracy scales inversely with the fourth power of the antenna aperture D_{elaa}, while that of the AoA estimation accuracy scales inversely with the square of the array aperture D_{elaa}. The typical near-field effect for range estimation can be seen in (19), where the same scaling law of the Fraunhofer distance $r_{\text{ff}} = 2D_{\text{elaa}}^2/\lambda$ with respect to aperture and wavelength is obtained for the inverse root-CRLB. Increasing the aperture D_{elaa} or decreasing the wavelength λ are beneficial to the accuracy of estimation, with the same impact as in r_{ff} of the two parameters. Moreover, the CRLB for AoA estimation has the same expression as that obtained under classical far-field conditions [11] and does not depend on the UE/target distance d. Thus, according to this analysis, no benefits are obtained in the near-field region for AoA estimation.

In summary, according to these results, the larger the number of antennas K (i.e., the aperture D_{elaa}), the better the accuracy of estimation, with a scaling law $\mathcal{O}(1/K^5)$ for the CRLB on range estimation and a scaling law $\mathcal{O}(1/K^3)$ for the CRLB on AoA estimation.

B. Bounds in the Geometric Near-Field Region

We now extend the analysis by accounting for ELAAs where the two approximations denoted in Sec. III-A and exploited for the CRLB derivation are not satisfied. In particular, here we consider the case where $d < D_{\text{elaa}}$, which is denoted as *geometric near-field* region [14]. In fact, such a boundary depends only on geometrical arguments and it is not related to the carrier frequency as it is for the definition of the Fraunhofer distance $r_{\text{ff}} = 2D_{\text{elaa}}^2/\lambda$. In this case, it is impossible to apply the Fresnel approximation, since its requirements are no longer fulfilled. In addition, the path loss at each antenna element must be considered separately. Therefore, in the following, we consider the original non-linear phase profile according to (11). In this case, we can compute the derivatives in (12) by obtaining[4]

[4]The other terms of the FIM are reported in the Appendix. The derivatives are calculated considering the dependence on $\mathbf{p}$ of the phase profile only according to (11). Thus, a performance bound is obtained for an estimator extracting location-dependent information solely from the phase term.

$$J_{dd} = \frac{8\pi^2 f_c^2 N\,\mathsf{SNR}_0}{c^2}\sum_k \frac{\left(1-\frac{x_k\sin\theta}{d}\right)^2}{\left(1+\frac{x_k^2}{d^2}-\frac{2x_k\sin\theta}{d}\right)^2}, \quad (21)$$

$$J_{\theta\theta} = \frac{8\pi^2 f_c^2 N\,\mathsf{SNR}_0}{c^2}\sum_k \frac{(x_k\cos\theta)^2}{\left(1+\frac{x_k^2}{d^2}-\frac{2x_k\sin\theta}{d}\right)^2}. \quad (22)$$

Observation 1: range estimation When the array size becomes extremely large, we can compute the limit for the FIM term J_{dd} in (21) as $K \to \infty$. For simplicity, by assuming a UE/target on the broadside direction of the array (i.e., $\theta = 0$), we obtain for the right-hand term in (21) the symmetric series:

$$\sum_{k=-\infty}^{\infty} \frac{1}{\left(1+a^2k^2\right)^2} \quad (23)$$

with $a^2 = \frac{\delta^2}{d^2}$ which converges to $\xi = \frac{\pi a\coth(\pi/a)+\pi^2\text{csch}^2(\pi/a)}{2a^2}$. Therefore, the information on the range saturates as the array becomes extremely large when considering the actual dependence on the non-linear phase term and path loss. Consequently, the related CRLB for range estimation necessarily presents a horizontal asymptote for large K, and is lower bounded as[5]

$$\mathsf{CRLB}^{(\hat{d})} \geq \frac{\lambda^2}{8\pi^2 N\,\mathsf{SNR}_0\,\xi} \approx \frac{\lambda^2\delta}{4\pi^3 N\,\mathsf{SNR}_0\,d} \quad (24)$$

where the approximation holds for small a (e.g., a standard $\lambda/2$ spaced array and practical UE/target distance). As can be seen, saturation of the performance occurs for ELAAs, and the saturation value depends on the UE/target distance d.

Observation 2: AoA estimation As for the range, when the size of the array becomes extremely large, we can calculate the limit for the FIM term $J_{\theta\theta}$ in (22) as $K \to \infty$. Assuming again $\theta = 0$, we obtain for the right-hand term in (22) the symmetric series:

$$\delta^2\sum_{k=-\infty}^{\infty} \frac{k^2}{\left(1+a^2k^2\right)^2} \quad (25)$$

which converges to $\xi' = \frac{\pi\delta^2\left(a\coth(\pi/a)-\pi\text{csch}^2(\pi/a)\right)}{2a^4}$. Therefore, even the information on the AoA saturates as the array becomes extremely large when considering the actual dependence on the non-linear phase term and path loss. Consequently, the related CRLB for AoA estimation necessarily presents a horizontal asymptote for large K, and is lower bounded as

$$\mathsf{CRLB}^{(\hat{\theta})} \geq \frac{\lambda^2}{8\pi^2 N\,\mathsf{SNR}_0\,\xi'} \approx \frac{\lambda^2\delta}{2\pi^3 N\,\mathsf{SNR}_0\,d^3} \quad (26)$$

where the approximation holds for small a. It is possible to notice that, differently from what predicted by the traditional expression (18), the accuracy limit does depend on the UE/target distance d.

[5]In fact, the inverse of the Fisher information on the range parameter (diagonal element of the FIM) equals the CRLB in the case all the other parameters are already known, or there is no correlation among the parameters to be estimated. Being the other parameters unknown cannot improve the estimation accuracy with respect to this case. Thus, any asymptote for $1/J_{dd}$ (here obtained for large apertures) represents a lower bound for the actual CRLB in the presence of other unknown parameters.

1) Impact of the approximations: In order to show what is the impact of the two approximations (i.e., Fresnel approximation and constant path loss approximation) separately, we repeat here the derivation considering the actual phase profile (without Fresnel approximation) but with a hypothetical constant path loss across the antenna array. In such a case, it is obtained for the two terms of the FIM concerning the range and AoA, respectively:

$$J_{dd} = \frac{8\pi^2 f_c^2 \, N \, \mathsf{SNR}_0}{c^2} \sum_k \frac{\left(1 - \frac{x_k \sin\theta}{d}\right)^2}{1 + \frac{x_k^2}{d^2} - \frac{2x_k \sin\theta}{d}}, \tag{27}$$

$$J_{\theta\theta} = \frac{8\pi^2 f_c^2 \, N \, \mathsf{SNR}_0}{c^2} \sum_k \frac{(x_k \cos\theta)^2}{1 + \frac{x_k^2}{d^2} - \frac{2x_k \sin\theta}{d}}. \tag{28}$$

By checking as before for the limits when $K \to \infty$, for range we have in the right-hand term of (27) the symmetric series:

$$\sum_{k=-\infty}^{\infty} \frac{1}{1 + a^2 k^2} \tag{29}$$

which converges to $\frac{\pi}{a} \coth(\pi/a)$. Differently, for AoA estimation, we have in the right-hand term of (28) the symmetric series:

$$\delta^2 \sum_{k=-\infty}^{\infty} \frac{k^2}{1 + a^2 k^2} \tag{30}$$

which does not converge. Therefore, saturation of the performance is mainly due to the adoption of the Fresnel approximation for range estimation and to the nonconstant path loss among the antennas for AoA estimation. This fact can be explained by observing the behavior of the phase profile for antenna elements far from the array center. According to the actual phase profile in (11), the phase is linear with x_k when $x_k \gg d$. Differently, by observing the series expansion for the distance term provided by the Fresnel approximation in (16), we observe a quadratic dependence with x_k, irrespective of the array element. Thus, the Fresnel approximation always leads to a non-linear phase term, which is required for near-field distance estimation, even though the wavefront is practically planar (i.e., linear phase) for the array elements far from the array center. This explains why no additional range information can be obtained, even in the case of significant amplitude for the associated signal, leading to a saturation of the performance. Differently, AoA does not require a non-linear phase profile for effective estimation; in fact, even in the far-field region, where the planar wavefront approximation holds, AoA estimation is feasible. In such a case, saturation occurs since the antenna elements far from the array center do not collect significant energy, thus do not contribute to the final estimation quality as far as the array becomes extremely large. Therefore, the linear SNR gain K in (17) and (18) is not experienced, and the traditional scaling laws with the array aperture size in (19) and (20) must be carefully considered. In particular, their validity is restricted to operation outside the geometric near-field region of the antenna array at the BS, i.e., for $d > D_{\text{elaa}}$. Numerical results of the following section will provide examples by comparing the CRLBs to the asymptotes described here.

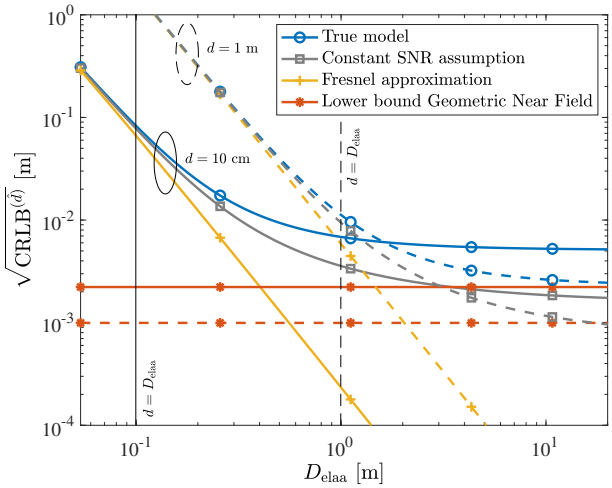

Fig. 2. Root-CRLB for range estimation as a function of the array aperture.

IV. Numerical Results

Simulations are performed considering a half-wavelength spaced array ($\delta = \lambda/2$), with $f_c = 28\,\text{GHz}$, an overall SNR at the reference antenna over the N subcarriers $N\,\mathsf{SNR}_0 = -20\,\text{dB}$, $\theta = 0$, and two different UE/target distances $d = 10\,\text{cm}$ and $d = 1\,\text{m}$.

In Fig. 2 the root-CRLB for range estimation is depicted as a function of the array aperture $D_{\text{elaa}} = (K-1)\delta$ (i.e., for increasing values of K). Continuous lines (–) are for $d = 10\,\text{cm}$ and dashed lines (- -) are for $d = 1\,\text{m}$. The blue curves (o) refer to the actual CRLBs derived with the FIM terms reported in Sec. III-B and obtained with the true phase profile and path loss model in the geometric near-field region; the gray curves (□) refer to the CRLBs obtained with a hypothetical constant path loss; lastly, the yellow curves (+) show the traditional CRLBs in (17) obtained according to the Fresnel and constant path loss approximations. For reference, the red lines (∗) are the lower bounds (asymptotes in (24)). It is possible to notice that traditional results based on the Fresnel approximation start to lose their validity when the array aperture becomes comparable to d, i.e., $d \approx D_{\text{elaa}}$ (see the vertical black lines). Indeed, the performance predicted according to the Fresnel approximation improves unbounded as the aperture increases, since all the antennas consider a non-linear phase profile for the received signal. This is not true when an ELAA is employed, as only the signal received by the central portion of the array exhibits a strong nonlinearity for its phase distribution. In contrast, when the true phase profile is adopted, we observe a saturation of the performance. The gap between the actual CRLB (blue lines) and the asymptotes (red lines) comes from the other unknown parameters. When a constant path loss is considered, together with the true phase profile, saturation is still experienced, as analytically shown in the previous section. In this case, the main impact on performance saturation comes from the right choice of the phase profile model.

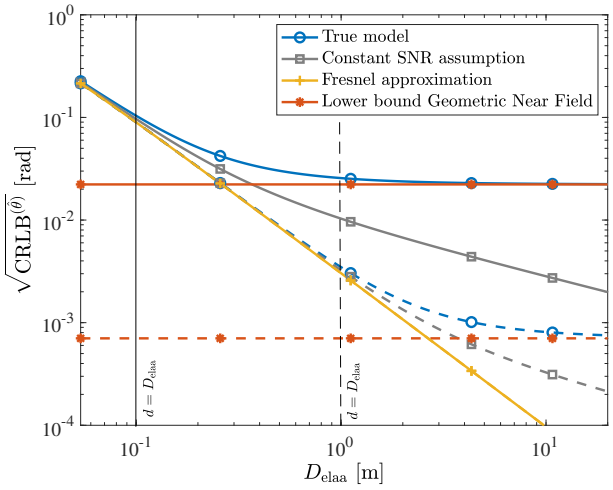

Fig. 3. Root-CRLB for AoA estimation as a function of the array aperture. UE/target distance of 10 cm (continuous lines) and 1 m (dashed lines).

In Fig. 3 results are reported for AoA estimation. In this case, when considering the classical CRLB in (18) obtained with the Fresnel approximation, the bound is independent of the distance d (yellow curves), and the accuracy improves unbounded as the array size increases. Differently, the bounds derived with the FIM terms reported in Sec. III-B, obtained with the true phase profile and path loss model in the geometric near-field region, show a saturation as predicted by the asymptotes in (26). Moreover, it is shown that the CRLB for AoA estimation becomes dependent on the UE/target distance, differently from what would be expected in far-field conditions or even in near-field conditions when $d > D_{\mathrm{elaa}}$. Notice that for the case $\theta = 0$ we are considering, the CRLB and the inverse of the information coincide, so that the lower bound in (26) predicts exactly the saturation value of the CRLB.

Notably, to attain the derived CRLBs, an estimator should account for amplitude variations along the ELAA by weighting each phase measurement according to the SNR at the corresponding antenna [15]. This gives greater influence in the estimation to phase values with higher SNR.

V. Conclusions

This paper has analyzed the performance limits for joint distance and angle estimation in the near field of ELAAs. The study highlights that the validity of traditional results derived under the Fresnel approximation and the assumption of constant path loss hold true as long as the array aperture remains small compared to the UE/target distance. However, as the array aperture approaches this condition (UE/target in the geometric near-field region), deviations become significant and performance saturation phenomena may occur. The findings provide novel insights into the fundamental limits for localization and sensing in near-field scenarios with ELAAs, emphasizing the need for refined models that account for varying path loss and phase effects over large apertures.

Appendix

The other FIM terms in the geometric near-field region are given as follows.

$$J_{\varphi\varphi} = 2\,N\,\mathsf{SNR}_0 \sum_k \frac{1}{f_k}$$

$$J_{\alpha\alpha} = \frac{2\,NK}{\sigma^2}$$

$$J_{\theta d} = -\frac{8\pi^2 f_c^2\,N\,\mathsf{SNR}_0}{c^2} \sum_k \frac{(x_k \cos\theta)\left(1 - \frac{x_k \sin\theta}{d}\right)}{f_k^2}$$

$$J_{\varphi d} = -\frac{4\pi f_c\,N\,\mathsf{SNR}_0}{c} \sum_k \frac{1 - \frac{x_k \sin\theta}{d}}{f_k\sqrt{f_k}}$$

$$J_{\varphi\theta} = \frac{4\pi f_c\,N\,\mathsf{SNR}_0}{c} \sum_k \frac{x_k \cos\theta}{f_k\sqrt{f_k}}$$

$$J_{\alpha d} = J_{\alpha\theta} = J_{\alpha\varphi} = 0\,.$$

References

[1] F. Liu *et al.*, "Integrated sensing and communications: Toward dual-functional wireless networks for 6G and beyond," *IEEE J. Select. Areas Commun.*, vol. 40, no. 6, pp. 1728–1767, Mar. 2022.

[2] H. Chen *et al.*, "6G localization and sensing in the near field: Features, opportunities, and challenges," *IEEE Wireless Commun.*, vol. 31, no. 4, pp. 260–267, Aug. 2024.

[3] Z. H. Shaik, E. Bjornson, and E. G. Larsson, "Cell-free massive MIMO with radio stripes and sequential uplink processing," in *IEEE Int. Conf. Commun. Workshops*, 2020, pp. 1–6.

[4] D. Dardari, "Communicating with large intelligent surfaces: Fundamental limits and models," *IEEE J. Select. Areas Commun.*, vol. 38, no. 11, pp. 2526–2537, Nov. 2020.

[5] E. Bjornson, O. T. Demir, and L. Sanguinetti, "A primer on near-field beamforming for arrays and reconfigurable intelligent surfaces," in *55th Asilomar Conf. Signals, Systems, and Computers*, 2021, pp. 105–112.

[6] H. Lu and Y. Zeng, "How does performance scale with antenna number for extremely large-scale MIMO?" in *IEEE Int. Conf. Commun.*, 2021, pp. 1–6.

[7] M. N. E. Korso, R. Boyer, A. Renaux, and S. Marcos, "Conditional and unconditional Cramér–Rao bounds for near-field source localization," *IEEE Trans. Signal Processing*, vol. 58, no. 5, pp. 2901–2907, May 2010.

[8] Z. Wang, X. Mu, and Y. Liu, "Performance analysis of near-field sensing in wideband MIMO systems," Feb. 2025. [Online]. Available: https://arxiv.org/abs/2404.05076

[9] H. Wang, Z. Xiao, and Y. Zeng, "Cramér-Rao bounds for near-field sensing with extremely large-scale MIMO," *IEEE Trans. Signal Processing*, vol. 72, pp. 701–717, Jan. 2024.

[10] M. F. Keskin, V. Koivunen, and H. Wymeersch, "Limited feedforward waveform design for OFDM dual-functional radar-communications," *IEEE Trans. Signal Process.*, vol. 69, pp. 2955–2970, Apr. 2021.

[11] S. M. Kay, *Fundamentals of Statistical Processing: Estimation Theory*. Prentice-Hall Signal Processing Series, 1993, vol. 1.

[12] A. Guerra, F. Guidi, D. Dardari, and P. M. Djuric, "Near-field tracking with large antenna arrays: Fundamental limits and practical algorithms," *IEEE Trans. Signal Processing*, vol. 69, pp. 5723–5738, Aug. 2021.

[13] B. Friedlander, "Localization of signals in the near-field of an antenna array," *IEEE Trans. Signal Processing*, vol. 67, no. 15, pp. 3885–3893, June 2019.

[14] N. Decarli and D. Dardari, "Communication modes with large intelligent surfaces in the near field," *IEEE Access*, vol. 9, pp. 165 648–165 666, Dec. 2021.

[15] N. Decarli, "On phase-based localization with narrowband backscatter signals," *EURASIP J. Adv. Signal Process.*, vol. 2018, no. 70, 2018. [Online]. Available: https://doi.org/10.1186/s13634-018-0590-4